Magnetic multilayers with (Nb,Mo,Cr) spacer materials

D. D. Koelling
Materials Science Division, Argonne National Laboratory, 9700 South Cass Avenue, Argonne, Illinois 60439-4845
(Received 27 December 1993; revised manuscript received 2 March 1994)

The properties of Nb, Mo, and Cr as the spacers in magnetic/nonmagnetic multilayers are examined. Utilizing the simple Ruderman-Kittel-Kasuya-Yosida-like response-function theory, one can elucidate not only which features of the bulk band structures are relevant but also discuss the implications of the spacers being inhomogeneously strained. The crucial question proves to be determining which caliper can resist all the broadening effects to appear actually as a macroscopic quantum effect. One mechanism is to minimize scattering by selecting wave functions with substantial s and p character. Another is to maximize the effective velocity and thereby minimize dephasing by the existing scattering. In Nb (110) and Mo (100), such considerations select Kohn-anomaly calipers which arise from the N-centered ellipses. Consideration of resilience to scattering effects is crucial to explaining why the Mo (100) repeat distance appears at three layers instead of at the two layers as seen in Cr. The uniform long repeat distances seen in Cr for the (100), (211), and (110) and the (110) repeat distance in Mo appear to be internally consistent in that they occur from the rim of the Δ centered lens surfaces and involve the strong mixing of t_{2g} and e_g d states. The analysis also suggests several factors which help to understand the systematics observed for spacers across the transition series.

I. INTRODUCTION

Artificial multilayers offer a new set of physical parameters to adapt the properties of materials. One very interesting feature[1] amongst the many already discovered is that in the magnetic/nonmagnetic layered systems, the magnetic layers — which are internally ferromagnetically (F) aligned — can be coupled in an antiferromagnetic (AF) arrangement across the nonmagnetic layers. This nonmagnetic material is often referred to as the spacer. The magnetic interlayer coupling oscillates between AF and ferromagnetic order as a function of spacer thickness[2] suggesting the sharpness of a Fermi surface is a critical feature which, in the simplest response theory, becomes a Ruderman-Kittel-Kasuya-Yosida (RKKY) type interaction.[3,4] As some of these systems exhibit a "giant" negative magnetoresistance anomaly,[5,6] they can be interesting as magnetic field sensors. Thus, there are two major problems to be considered for these systems: "What are the essential features of the interlayer magnetic coupling?" and "What is the nature of the giant magnetoresistance?"[7–9] Here, we are interested in the former.

To attempt some theoretical understanding, there are two ways of proceeding and, quite naturally, both avenues are being explored. One approach selects representative cases on which detailed electronic structure calculations are performed and then dissected.[10–15] Because these materials involve layer thicknesses of at least mesoscopic — if not macroscopic — size, one must be prepared for a heroic effort and then be careful that the calculations are numerically significant. The real worth of the calculation must come from the final detailed analysis as a representative case of a statistical ensemble — rather than agreement with experiment. In recognition of the utility of this approach, it should be noted that it yielded the earliest prediction of antiferromagnetic coupling.[16] The alternate approach is to define simpler models hopefully capturing the essential features and consider their properties (as is the case of the original RKKY interpretation). Of course, rather than competing approaches, they must be used in concert both with each other and with further experiments if we are to hope to make progress.

So what are the essential features of a model worthy of examination? First, the basic unit can be reduced to a single spacer layer between two magnetic layers (see Fig. 1), although the true experimental system often involves arrays of interspersed magnetic and spacer layers. The properties of the repeated systems can be built up on those of the isolated unit, and so initially it is only necessary to consider this simpler system. (Unless one wishes to exploit periodicity — this is an easy way to discuss the so-called aliasing effect.) And, because the magnetic layers are "thick" and their actual thickness has comparatively little effect, they can be considered semi-infinite solids. Inserted between the magnetic layers are two interfaces and the spacer. The interfaces are the regions where the intermixing and imperfections (referred to as surface roughness) occurs, lattice mismatch strains are hopefully accommodated, etc. Although one may question how fast the strain effects die away as one proceeds into the spacer,[17] the major charge effects can be hoped to screen out within a few atomic layers. So the interfaces can be viewed as being of finite extent leaving the interior of the spacer much as it would be in a bulk solid. The interfaces are generally idealized to a sharp interface or one where the roughness is represented by substitutional intermixing of two atomic layers.[18,19] See

0163-1829/94/50(1)/273(18)/$06.00

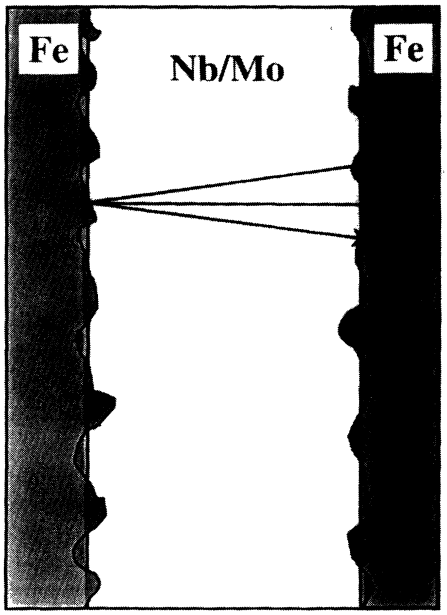

FIG. 1. Schematic representation of the multilayer system. Two layers of iron are coupled through the Nb/Mo spacer — which is initially viewed as a simple transmission medium. The boundaries, which are generally not perfect, are approximated as perfect interfaces to which corrections are applied. The figure misrepresents the relative size of the length scales for the variations along and perpendicular to the interfaces. One can expect the scale along the interface to be longer than shown. Not represented are the larger-scaled imperfections such as interdiffusion and strains.

Fig. 1. On the other hand, the interface structure is crucial to the enhanced magnetoresistance[20,21] that is a primary factor driving interest in these systems. The approach used by van Schilfgaarde and Herman[22] would appear to be especially useful for looking into the interface effects although full Green's function matching techniques[23] would be better.

One expects to be dealing primarily with magnetic changes in the central regime of the spacer that are minor deviations from the bulk. This is strongly supported by the successes of the non-self-consistent calculations for such systems.[24,22] This in turn motivates the use of a response theory treatment on the bulk material for the internals of the spacer — at worst only incorporating enhancements, nonlinearity, and/or finite size quantization effects which is the way one might view the Green's function based calculation of Mirbt *et al.*[25] Because the ferromagnetic material is internally ferromagnetically coupled, the response function is driven by the interactions at the interface and this has significant consequences. This view underlies all model treatments whether the model applied is truly a response formulation as the RKKY,[3,4] focuses on spin-flip currents,[26] or concentrates on the boundary effect as the driving force.[17,27–31] The essential parameters taken for the first analysis are the critical spanning vectors that have been extensively used in Kohn-anomaly analyses[32] and the local joint density of states at those spanning vectors. Because the local joint density of states involves the comparison of band slopes and curvatures at the two end points of the spanning vector, it is presented as a special effective mass parameter. But it should be remembered that it is the simple state density for the transition unweighted by the matrix elements that would appear in a perturbation expression. As with all such "generalized" response function analyses (optical, x-ray, susceptibility, dielectric, etc.) the positions are generally well determined but strengths are poorly represented.

Much success has been obtained applying the Fermi surface driven models to systems with copper spacer layers. These Co/Cu systems[33–36] and Fe/Cu systems[37,38] provide a spacer with a simpler electronic structure where there are only very few spanning vectors so selection is not an issue. The success of these studies, and those for the other simple metals,[39] clearly establishes the significance of the Fermi surface for such phenomena. The copper spacer offers some special opportunities as well. Noble metal films on a magnetic substrate have been the premier systems in which to demonstrate the formation of quantum well states.[40–42] The formation of such states offers a significant mechanism to sharpen the coherence of the response thereby enabling the longer ranges of the AF interaction. Also, epitaxial coupling can drive the Cu to exist in the bcc crystal for 10–11 monolayers[37] giving a different view — but only if the Fe thickness is much larger than the Cu thickness.

In this paper, the interest will be focused on systems with VB and VIB elements used as spacers specifically examining what can be learned viewing the spacer as a transmission medium. These materials have multiple Fermi surface sheets with complex shapes with the consequence that there are many possible Kohn-anomaly spanning vectors which might give rise to magnetic repeat distances. It was this issue that initiated my efforts on this project. The intent was merely to show that tabulating the Kohn-anomaly spanning vectors gives an extensive list of possible repeat distances which included the one or two actually observed. In Sec. II, a brief discussion is given of the significance of the Kohn-anomaly vectors and associated effective mass parameter (joint density of states) as it arises from the simplest response function analysis. Then the Kohn anomalies are then presented using plots of the same form as used to discuss phonon anomalies.[32] This is also the presentation form used by Stiles,[31] who has performed an exhaustive survey of these spanning vectors. It is seen that, indeed, the observed frequencies can be related to Kohn anomalies but also that it will be seen to be very nearly devoid of significance. The exception is that it enables one to determine which parts of the Brillouin zone (BZ) are involved. This, however, is useful because it reveals the associated wave function character. That information will be used below to suggest the hypothesis that the mixing of the e_g state associated with the body of the Γ centered jack and the t_{2g} state associated with the knob has a special significance. That mixing is responsible for forming the Fermi surface into the jack with the lens inside. The resulting mixed state character on the rim of the lens can be related to the long period oscillations in Cr (100), (110),

and (211) directions and also to the observed repeat distance for Mo (110). As for the predictive power of the local joint density of states mass parameter, Stiles has observed that the correlation of observed repeat distance to the strength of the mass term (local joint density of states) is quite weak. I would go further and state that, in these *d*-state materials, it is essentially nonexistent. It is this observation that drives one to look deeper. What one then rediscovers is the importance of asking for any macroscopic quantum phenomenon how the quantum effects survive to the macroscopic regime.

The simplest-possible modeling neglects the fact that these artificial structures are *not* perfect. The initial acknowledgement of this fact has been the recognition that interface roughness will suppress the shorter wavelength repeat distances. A primary concern here will be that greater levels of imperfections need be considered: The strains of the imperfect lattice match, the layer spacing fluctuations driven by the work function mismatch, the granularity of the spacer, and impurities are all significant. To explore this, the techniques of early transport and susceptibility calculations can be employed on the simple response function modeling. These are based on the assertion that the *s-p* states carry the long-range information as the *d*-states are more rapidly dephased by the scattering.[43] A scattering mechanism has been successful in dealing with rare earth RKKY interactions,[44–48] and so this is not unreasonable. As will be seen in Sec. III, significant information can be obtained from a simple simulation. In these materials, the Fano antiresonance acts to severely reduce the *s-p* character at the Fermi energy. By assuming that coherence can only be maintained when coupling states with significant *s-p* character, nearly all spanning vectors are eliminated from consideration leaving only those couplings involving the ellipses located about the point N in the BZ. Because the Fermi surface in the noble metals has a strong admixture of *s-p* character, one can expect that they will not be as significantly influenced by the greater *d*-state scattering and that this effect would not be so pronounced. Thus, the successes found in Cu are actually consistent with this view rather than precluding it.

One's initial impression is that Cr should be viewed as the control. The Fe/Cr system[1,2,5,6,49–51] and Co/Cr system,[2,53] with Cr acting as the spacer, have been studied extensively. Of course, for Cr to be viewed as a nonmagnetic spacer, the Cr spin density wave should be suppressed.[50] The strong response associated with the spin density wave must still be present, however, and it can give rise to oscillatory behavior with a two-monolayer (ML) repeat distance. When the interfaces between layers are of high quality, this short wavelength oscillation is indeed observed using a technique involving a wedged-shaped spacer.[51] On the other hand, when the layer interfaces are rough, the rapid oscillation is suppressed (it can be reintroduced by annealing the interface[52]) and only a longer wavelength oscillation is observed: At 18 Å, this wavelength is unusually long. It also has the interesting property of occurring at precisely the same repeat distance, phase, and strength for both the (100) and the (211) directions[54] and probably also for the (110) direction as well.[56] Although this work was not specifically designed to study this problem, it does suggest an interesting hypothesis focusing on the wave function mixing in the rim of the lens. Because of the expected incipient antiferromagnetism, a question that may be fruitfully asked is whether a low order response theory is adequate or whether the system has so dramatically responded as to require a fully self-consistent treatment. Interface-partial-self-consistent calculations[22] strongly suggest it is not crucial. Besides the incipient antiferromagnetism of Cr, there is another important feature that contributes to the successes found using this spacer: It is a much more stably formed, much better lattice matched, and thus more nearly crystallographically perfect system than most.

Exploring the isoelectronic systems varies more parameters in multilayers than in bulk because the spacer must still be connected to the same magnetic layer. Thus, variations in adhesion, diffusion, and lattice mismatch also become significant. Replacing Cr by Mo has proven an instructive exercise. The longer wavelength oscillation is also observed for isoelectronic Mo,[55] but in the (110) direction. It occurs at a wavelength (11 Å) more consistent with the general observation that the rough-interface systems typically exhibit wavelengths in the range 9–11 Å.[56] Using the wedge technique for Fe/Mo in the (100) direction, the shorter wavelength oscillation appears[53,57] but at 3 ML rather than the 2 ML that might be expected from the generalized susceptibility peak (possible incipient spin density wave).

It would be very interesting to see what would happen in the Fe/Nb system could the Nb be driven superconducting thereby creating a gap at the Fermi energy. Unfortunately, the moments in the Fe layers are too effective at pair breaking. No superconductivity is seen unless the Nb is too thick to be interesting. Instead, normal transition metal behavior is observed with a repeat distance of 9 Å when the Nb is textured in the (110) direction.[59] For Co/Nb, the antiferromagnetism is reported to be too weak to observe a period although a first peak is observed at a slightly smaller Nb thickness.[56] Since this first peak position is dependent on phase and the phase depends on magnetic layer composition, one must assume the same repeat distance as the Fe/Nb system. This is found to be the case in numerous systems. Co/V is found to have a similar 9 Å repeat distance.[56]

There are a number of features that one would like to understand. The primary question is what determines which of all the many Kohn-anomaly points actually appears experimentally. There is another lesser question, of course, as to whether all observed repeat distances do in fact correspond to such points. That, however, has pretty well been resolved and these materials, with their dense populations of possible points, can say little about that question. Only when the interfaces are of high quality are the shorter repeat distances observed which has successfully been attributed to removal of the effects of surface roughness. In Cr, this shorter wavelength appears at a distance of two monolayers (ML) consistent with the spin density wave instability there. But in the case of isoelectronic Mo, it appears at roughly 3 ML.

Why should this be? When the interfaces are rough, the repeat distances appear to universally occur in the 9–11 Å range — Cr and Os[58] are exceptions at 18 Å and 15 Å. Is this an indication of some fundamental aspect of multilayers or a simple consequence of measurement factors? Clearly, the shortest repeat distances are suppressed by surface roughness. They are further suppressed by the rapid dropoff of the *d*-state form factors as will be discussed in Sec. II. At the other end of the spectrum, the very long distances are difficult to observe because the signal has seriously decayed by the time one reaches the distances necessary to observe them. An important question is whether that is enough to explain the observed narrowness of range. It will be argued that scattering mechanisms which operate to select the *s-p* character will also act to favor repeat distances in that range.

The dependence of the coupling strength decay on increasing spacer thickness can be informative. Unfortunately, the indeterminateness of the boundaries makes it hard to extract firm functional dependences. If the oscillatory behavior were to be driven by a peak in the generalized susceptibility, the oscillations would show an Gaussian decay with a decay length inversely proportional to the width of that peak. The z^{-2} dependence used by Parkin[56] in his analysis arises from the dephasing around a Kohn-anomaly *point*. If instead the coincidence were to occur along a line, it would give an $z^{-3/2}$ dependence for that $\mathbf{q}$ vector. Full planar nesting would give a z^{-1} dependence. In addition to these phase coherence factors, a finite mean free path occurring for the coupled states would also give an exponential decay to the dependency. Thus, it might be possible to garner information from the form of the decay if it could be reliably determined.

On the other hand, I would argue that the phase is not as informative at this time. Again, the fuzziness of the boundaries seriously undermines the significance of any small differences. And whether the initial ordering is ferromagnetic or antiferromagnetic is a consequence of the near neighbor interaction between the ferromagnetic ion (Fe, Co, or Gd) and the first spacer ion.

II. SIMPLEST VIEW

The question of initial interest to us in this project was just how dominant the spacer Fermi surface was in determining the repeat distances. The simplest model emphasizing that aspect is the RKKY model. The simplicity of the model will be exploited in the next section to discuss scattering effects. The model must first be converted to one in which the magnetic layers serve as transmitter and receiver of magnetic information at the interface so that the focus can be on information transmission through the spacer layer. As a first approximation, the spacer is viewed as a passive transmission medium and is assumed unaffected by its new environment except for population realignments. As a consequence, the bulk band structure can be used to calculate requisite response functions. The magnetic layers are taken to be perfectly ferromagnetically aligned internally so that they can be described by a single spin orientation and interaction at the interface. Also as an initial approximation, one assumes perfect lattice matching so that sums are performed on the lattice of the spacer. A highly desirable benefit of assuming perfect lattice matching is that one can then work in a reduced zone scheme and introduce the notation that any δ function present actually represents a lattice sum of δ functions. This significantly reduces the complexity of any discussion of aliasing. However, the assumption that the interaction need only be considered with the first layer of the magnetic material has significant implications as to what is an equivalent vector, as will be discussed below. The model neglects much: mismatch strains, work function mismatches (i.e., charge transfer), interface roughness, interdiffusion, self-consistent relaxations, possible formation of bound or resonant states, and possible quantum well states to name only a few. It is the simplest possible view of the problem and, while not the whole truth, is simple enough to be easily comprehended — thereby a useful basis on which to build understanding.

A. Basic response theory

The discussion will follow Bruno and Chappert[4] but introduce a slightly different view and some minor improvements. Its main function is to establish notation and background, and then provide the basis for a simple incorporation of effects arising from the system being imperfect. To obtain the interaction of the two magnetic layers across the spacer, the model sums RKKY pairwise interactions of site i in the surface of one magnetic layer with site j in the other. The exchange interaction is

$$J(\mathbf{R}_{ij}) = \frac{-1}{2(2\pi)^6} \int d\mathbf{q} e^{i\mathbf{q}\cdot\mathbf{R}_{ij}} \sum_{n,n'} \int d\mathbf{k} \frac{|M_{\mathbf{k}+\mathbf{q},n';\mathbf{k},n}|^2 \, [f(\epsilon_{\mathbf{k},n}) - f(\epsilon_{\mathbf{k}+\mathbf{q},n'})]}{\epsilon_{n'}(\mathbf{k}+\mathbf{q}) - \epsilon_n(\mathbf{k})}, \quad (1)$$

where ϵ is the band energy and f the Fermi occupation factor. The sum on $\mathbf{k}$ extends over the entire Brillouin zone and the periodicity is accounted for through the standard treatment of the reduced zone scheme. The n and n' sums ideally extend over all bands and are quite slowly convergent. However, only those bands at or very near the Fermi energy actually contribute significant structure — in fact, the entire discussion focuses on the Fermi energy. Since the overall constant value has no influence of interest to us here, this is no problem. The interaction matrix elements in Eq. (1) will have contribution only from the interface and have the $\mathbf{S}_i \cdot \mathbf{S}_j$ dependence removed and explicitly displayed in the pair-interaction Hamiltonian. It is the approximate treatment of the matrix elements that permits separating the problem into considerations of the spacer material as a trans-

mission medium with the interfaces as transmitter and receiver of that information. The matrix element is often taken as $\mathbf{k}$ independent, and so its contribution can be taken outside the $\mathbf{q}$ integration but that is not necessary. In actual application, one focuses only on the Kohn-anomaly caliper points to deal with the oscillatory magnetic behavior which selects a small set of $\{\mathbf{q},\mathbf{k}\}$ values, and so neglect of the $\mathbf{q}$ dependence of the coupling terms is more neatly done in practice. Actually, one would like to put things in the form $|M|^2 \Rightarrow \zeta(i)\zeta(j)$ which requires that one use the fact that the two magnetic moments are well separated and explicitly consider the difference between a parallel and antiparallel alignment. Such an (approximate) procedure can actually accommodate the fact that these matrix elements are an exchange interaction and not just an interaction with a perturbing potential. Then

$$J(\mathbf{R}_{ij}) = \frac{-\zeta(i)\zeta(j)}{2(2\pi)^3}\int d\mathbf{q}\tilde{\chi}(\mathbf{q})e^{i\mathbf{q}\cdot\mathbf{R}_{ij}}, \qquad (2)$$

where the generalized susceptibility $\tilde{\chi}$ is that of the spacer and ζ is the form presumed for the interaction with the magnetic ion. ζ has been dealt with in a variety of ways. Yafet[3] used an experimental factor extracted for Gd for Gd-Y superlattices; Bruno and Chappert[4] utilized a contact interaction for Fe-[Cu,Ag,Au]; Wang *et al.*[18] utilized an *s-d* interaction model for Fe-Cr but with the Fe *d* states approximated at a constant energy; and Bruno[27] utilized an *s-d* mixing model treated using Green's function techniques (this should be the same model as that of Hasegawa[14] but treated differently) which summarizes the *d*-state energy as virtual bound states locally for each $k_{\|}$. One could also map the surface reflection factors used in quantum well models[31,28] into this form. To proceed, we need only use the form of the interaction is often reduced to a simple on-site interaction as expressed in Eq. (2). One can then incorporate the question as to the exact form of the interaction into the factor (Z) defined below to simulate the complications of the true interface. However, several comments are in order. This approach has used linear response to isolate the spacer effects from the interface effects. It is appropriate only for weak coupling which very well may not be the case in many systems. It must absorb the local interactions such as an antiferromagnetic superexchange[60] or simpler *d-d* near neighbor coupling into the interface term.

The generalized susceptibility $\tilde{\chi}(\mathbf{q})$ is the simplification of the noninteracting susceptibility

$$\chi(\mathbf{q}) = \frac{-1}{(2\pi)^3}\sum_{\mathbf{k},n,n'}\frac{|\langle(\mathbf{k}+\mathbf{q}),n'\,|e^{i\mathbf{q}\cdot\mathbf{r}}\,|\mathbf{k},n\rangle|^2[f(\epsilon_{\mathbf{k},n}) - f(\epsilon_{\mathbf{k}+\mathbf{q},n'})]}{\epsilon_{n'}(\mathbf{k}+\mathbf{q}) - \epsilon_n(\mathbf{k})}, \qquad (3)$$

obtained by setting the $e^{i\mathbf{q}\cdot\mathbf{r}}$ matrix elements to one such that it only represents phase space effects. In this case, the generalized susceptibility appears because the matrix elements that should occur in Eq. (1) for the multilayer system involve contributions only within the interfaces and we are contriving to separate out the spacer contribution. As is quite common with such "generalized" approximations, this will seriously restrict any prediction of relative strengths. Given a usable form for the interface interaction terms, one would pull them out of Z and put them in $\chi(\mathbf{q})$ as a more accurate response function. One can get some ideas of general trends by noting that the approximate matrix elements used in a linear combination of atomic orbitals (LCAO) calculation of the susceptibility[61] are actually a simple on-site form factor. Thus, the same approach should apply to Z more or less consistent with the discussion of Herman and Schreiffer[62] implying that one should be concerned with the form factor of Fe such as shown in Fig. 2. If this much simplified consideration is the dominant effect, then Z must be a rapidly decreasing function of $\mathbf{q}$. The effect is all the more pronounced since the form factor enters the matrix element as a product and Z contains the matrix element squared so the variation of Z would go as the fourth power. To get a "number" for a perturbing potential term from Fig. 2, one must use a knowledge of the wave function so that the L=0 term can be combined with L=2 and L=4 terms multiplied by the orbital dependent angular factors given in Table I of Callaway *et al.*[63] To be semiquantitative, one might worry about taking the angular decomposition from the spacer wave function information, but that is a very dubious approach since the actual matrix elements involve an exchange interaction and not just a perturbing potential. Arguments based on null matrix elements due to the angular terms should be considered of less reliability than the drop off due to form factors. However, except at large Q, the higher L terms are too small to affect the qualitative observation

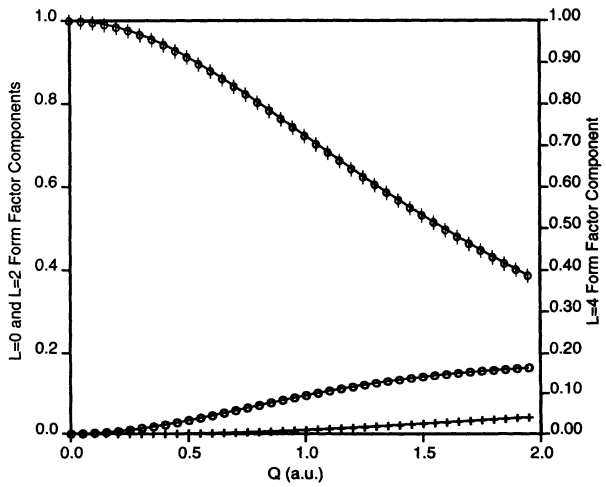

FIG. 2. Fe *d*-orbital form factor. The L=0 (slashed O), L=2 (O), and L=4 (crosses — scale at right) *d*-orbital form factors. Q is given in atomic units: $\left(\frac{\pi}{a}\right)$ is 1.15 for Cr, 1.06 for Mo, and 1.01 for Nb.

that the form factor drops significantly with increasing Q.

The analysis proceeds[4] by seeking the interaction-strength factor I obtained when the cosine of the angle between the moments (the remnant of the spin scalar product of the RKKY Hamiltonian) is extracted from the energy per unit area. One looks for oscillations in the sign of I with increasing thickness of the spacer. I involves the double sum over magnetic sites i and j in the two surfaces of the interacting magnetic layers. If one identifies the plane of the Fe interface as the atomic plane containing an adequate number of Fe atoms (in the perfect idealized case considered here, the last plane of Fe atoms) and calls the separation of the two planes z, then one can write

$$\mathbf{R}_{ij} = \mathbf{r}_{1i} + z\hat{\mathbf{z}} + \mathbf{r}_{2j}\,, \tag{4}$$

which isolates the layer thickness from the displacements within the layers. $\mathbf{q}$ is separated into its components perpendicular and parallel to the planes:

$$\mathbf{q} = q_z\hat{\mathbf{z}} + \mathbf{q}_{\|}\,. \tag{5}$$

Then, replacing ζ by a suitable average value, the site sums involving $e^{i\mathbf{q}_{\|}\cdot\mathbf{R}_{ij}}$ for the interaction strength can be isolated and performed giving

$$I(z) = \int d\mathbf{q} Z(\mathbf{q})\tilde{\chi}(\mathbf{q})e^{iq_z z}\,, \tag{6}$$

where all constants have been absorbed into $Z(\mathbf{q})$, whose primary function is to represent the coupling effects at each interface. It should be recognized that $Z(\mathbf{q})$ encapsulates (or hides, according to ones thinking) a significant part of the problem. Assuming perfect periodic interfaces, one of the two summations present in Z is a simple average of the nontrivial sum on the relative [two-dimensional (2D)] dispacements in the planes $(\mathbf{r}_{2j} - \mathbf{r}_{1i})$. For the perfect lattice matching approximation with perfect interfaces, Z is a weighted sum of δ functions on the lattice in the plane. Any deviation from the ideal model would introduce broadenings, possible superlattice points, and structure factors. If one uses a contact potential approximation and considers the random occupation by the magnetic atoms of the sites of two planes at the interface,[18,19] a term of the form $[A + B\cos(\phi)]$ is introduced. $\cos(\phi) = -1$ at the large q boundary of Eq. (6), and so this factor will act to suppress response in that region. This factor is a significant part of the reason rough interfaces suppress short period oscillations. Generally, this roughness across n layers will act as a short wavelength filter suppressing coupling to the magnetic layer for wavelengths shorter than n layer spacings. When the structure of the matrix elements is considered, roughness can have even more profound effects especially when more than simple subsititutional disorder is present.[62] Lattice mismatch will produce strain fields, dislocations, and defects extending into the bulk of the layers. Thus, these effects must appear not in $Z(\mathbf{q})$ but $\tilde{\chi}(\mathbf{q})$ which will be done below using simple modifications of the formalism to account for their scattering.

B. Brillouin zone reconstruction: An observation

One simplifies the problem significantly by separating the in-plane from the cross-plane ($\hat{\mathbf{z}}$) effects in the integrations. This is done by choosing to use a more convenient, but entirely equivalent, BZ to do the $\mathbf{q}$ integrations and isolate $\mathbf{q}_{\|}$. Because the multilayers are based on crystalline atomic planes of separation d, it is very useful to choose the BZ to be a prism bounded by the planes at $\pm\pi/d$. Because the planes are crystalline planes, one can then make the standard constructions — but in 2D — to deal with the in-plane coordinates. The $\mathbf{q}_{\|}$ integration in Eq. (6) can then be readily done which will select $\mathbf{q}_{\|} = 0$ modulo a reciprocal lattice vector in the plane. With this result, and simultaneously converting to a real integral, one obtains

$$I(z) = \int dq_z \bar{Z}(q_z)\tilde{\chi}(q_z)\cos(q_z z)\,. \tag{7}$$

So the geometry has selected the perpendicular component of the susceptibility, as pointed out by Yafet.[3]

This BZ reconstruction, however, reveals another very interesting feature of the geometry of the problem. In this construction, the lattice is being viewed as a stacking of planes which are more open than their separation d. Because of this, the primitive translations within the plane are smaller than for the 3D lattice, increasing the number of equivalencies occurring. This can be made clearer by discussing specifically the three directions considered here. In the (001) direction, the bcc crystal is made up of a stacking of simple square lattice planes whose primitive translations would be $\frac{\pi}{a}(100)$ and $\frac{\pi}{a}(010)$ for the cross-plane direction being the $\hat{\mathbf{z}}$ direction. The 2D BZ is the square bounded by $\pm\frac{\pi}{a}$ in the x and y directions. q_z is bounded by $\pm\frac{\pi}{d} = \pm\frac{2\pi}{a}$ so the unit cell volume is $2\left(\frac{2\pi}{a}\right)^3$ as required. Note what happens for a $\frac{\pi}{a}(202)$ reciprocal lattice vector (umklapp-type process). Because the $\frac{\pi}{a}(200)$ is a primitive translation in the plane, the line $\frac{\pi}{a}(2,0,2+q_z)$ maps onto the $\hat{\mathbf{z}}$ line *but as the mirror image* because $0 \rightarrow \frac{2\pi}{a}$ occurs for q_z traversing $\frac{2\pi}{a} \rightarrow 0$ when the reflection symmetry is considered. For the (110) direction, the planes are made up of face-centered rectangular lattice of ratio $\sqrt{2}$ to 1. The 2D reciprocal lattice vectors are $\frac{\pi}{a}(1,\bar{1},2)$ and $\frac{\pi}{a}(1,\bar{1},\bar{2})$. q_z runs between the N points $\pm\frac{\pi}{a}(1,10)$. Here again a (022) 3D reciprocal lattice vector coupled with a $(1,\bar{1},\bar{2})$ 2D plane vector results in the mirror image being equivalently mapped onto the $\mathbf{q}_{\|} = \mathbf{0}$ line. For the (211) direction, the planes are rectangular lattices with primitive translation vectors $\frac{a}{2}(1,\bar{1},\bar{1})$ and $a(0,1,\bar{1})$. So the reciprocal lattice generators are $\mathbf{K}_1 = \frac{4\pi}{3a}(1,\bar{1},\bar{1})$ and $\mathbf{K}_2 = \frac{\pi}{a}(0,1,\bar{1})$. d is $a/\sqrt{6}$, and so $\mathbf{q}$ ranges to $\pm\frac{\pi}{a}(211)$. Again $\frac{\pi}{a}(220) - \mathbf{K}_2 = \frac{\pi}{a}(211)$, and so one has the same mirror mapping of $(211) - \mathbf{q} \rightarrow \mathbf{q}$. For the perfect lattice matched system, the remapped $\mathbf{q}$'s discussed for each direction actually remap into what one started from because of the surface terms in Z. Because $\mathbf{q}_{\|} \neq \mathbf{0}$ and the adjacent planes do not line up, Z contains a factor which fluctuates between ± 1 for the (100) and (110) directions. This is equivalent to the "missing"

component of the **q** vector bringing one back to where one started from. The situation is more complex but to the same effect for (211). However, the situation is interesting because the Z contribution can get filtered out. In the ideal model, this can happen because the magnetic ion locally influences the first layer of the spacer. That is quite credible since different magnetic materials can change the phase by π. Then, once one considers a rough surface, this term should appear with a factor comparable to the loss of strength for **q**'s near the boundary of the BZ.

C. Band structure and generalized susceptibility

The generalized susceptibility $\tilde{\chi}(\mathbf{q})$ is the focus of the discussion of the spacer contribution. Yafet,[3] in discussing the rare earth system Gd/Y, utilized calculated values of $\chi(q)$ which actually exhibits a somewhat sharp peak dominating the behavior at the range of distances considered. Such a peak yields oscillatory behavior but decays exponentially (actually, Gaussian) at a rate proportional to the width of the peak. The generalized susceptibilities for Nb, Cr, and Mo resulting from the inclusion of the first five bands are shown in Figs. 3 and 4.

Before discussing them, a brief statement is needed concerning the band structures that will be used throughout. Self-consistent calculations were performed for each material using linearized augmented plane waves (LAPW's) at the level of a warped muffin tin (WMT) shape approximation. The Hedin-Lundqvist parametrization[64] was used to represent the exchange correlation. The bands were then obtained at 130 points ($\pi/4a$ cubic mesh + centers of tetrahedra of twice breaking up the irreducible wedge + 11 sensitive points on the symmetry lines). These were then spline fit[65,66] using 560 star functions to produce the representation of the bands actually used throughout this investigation. The spline fitting was done with the energy scale adjusted to the average energy of each band. This very simple approach is actually equivalent to the more elaborate procedure originally proposed[67] to handle the fact that the spline fit minimizes the size of the $\mathbf{K} = \mathbf{0}$ coefficient. The generalized susceptibility was then calculated using the analytic tetrahedron scheme.[68] Because the interest is in the Fermi surface properties, Nb requires special attention. Nb (and Cr) lies at a critical juncture in terms of the relative population of the d states versus the s-p states[69] so that it is particularly sensitive to the nonspherical self-interaction effects.[70,71] An effective empirical correction is to artificially shift the d's relative to the s-p's.[72] Interestingly, smoothing shape approximations very nearly mock up this effect so that the requisite artificial shift is nearly zero when making the muffin tin shape approximation while it is at least 20 mRy when using a general potential.[73] The original general potential calculation was performed for an exchange-only potential — otherwise the requisite correction would have been larger. In the case of the WMT shape approximation and and exchange-correlation functional, it was found that a 10 mRy shift optimized the agreement of the calculated Fermi surface with the de Haas–van Alphen (dHvA) data. This empirical adjustment brings a remarkable range of properties into line,[74] and so its use here is strongly motivated.

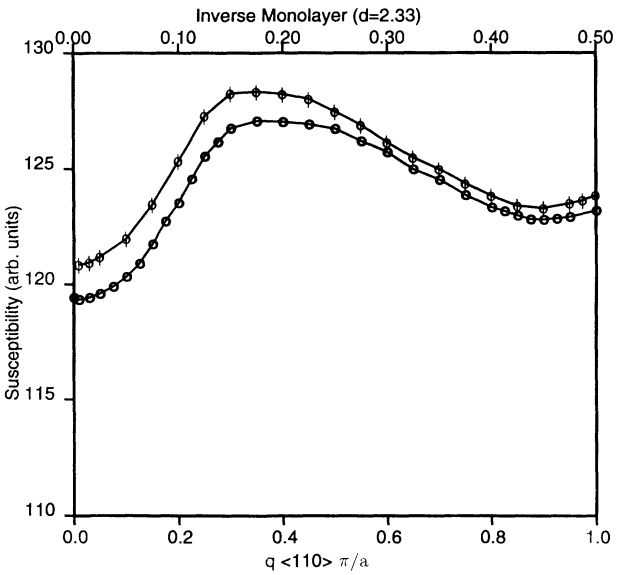

FIG. 3. Generalized susceptibility $\tilde{\chi}(\mathbf{q})$ for Nb along the (110) direction. The two separate results are calculated with (slashed points) and without the empirical adjustment discussed in the text. As seen in the generalized susceptibility, the d-p shift merely produces a slight increase in the overall susceptibility without much change in the structure. The observed peak occurs at and below the **q** value associated with a 9 Å (4 ML) repeat distance. Its width, however, would imply a very rapid Gaussian decay of the coherence. For convenience, a **q** coordinate in terms of inverse layers has been included on the top of the plot.

One can quickly demonstrate that the generalized susceptibility gives only very little insight. The group VB representative, Nb (110), does show a weak, broad peak in $\tilde{\chi}(\mathbf{q})$ roughly in the vicinity of the observed repeat distance although at somewhat smaller **q**. (See Fig. 3.) However, the breadth of that peak would imply a very rapid decay. The other minor structure occurring at the Brillouin zone boundary (2 ML repeat) does not relate to any experimental observation. The relevant generalized susceptibilities for the group VIB elements are shown in Fig. 4. The most useful result is to the strong peak near, but not quite at, the zone boundary in the (100) direction. This is the peak associated with the spin density wave of Cr. The matrix elements that do not appear in this model would nearly remove this peak for the susceptibility[61] so that it is necessary to include the exchange enhancement to actually get the spin density wave to appear in a response function calculation.[75] Also present are a very weak maximum near the center of the zone, a maximum just beyond the halfway point, weak structure at a **q** slightly larger than for a 3 ML repeat distance, plus some other very weak structures comparable to that appearing near the zone center. They are

all broad peaks, and so they should decay quickly were they to be seen. There is little evidence for the long 18 Å repeat distance unless one is willing to focus on the shoulder of the structure at Γ. The results for Mo in the (100) direction look very much as those for Cr except scaled down a bit. One would not be able to determine from these data that Cr and Mo behave differently as spacers. The maximum occurring near $\mathbf{q} = \mathbf{0}$ for Mo would be more convenient were it to occur in Cr instead of the shoulder but one could hardly take such structure as a serious prediction. It is suggestive that the structure just above the $\mathbf{q}$ for a 3 ML repeat distance has sharpened and moved down closer to the 3 ML point since only this 3 ML repeat distance is actually observed. The only structure in the (211) direction for Cr is a prominent shoulder near $\mathbf{q} = \mathbf{0}$ and a weaker one near the outside boundary. The dropoff of the $\mathbf{q} = \mathbf{0}$ shoulder starts below the $\mathbf{q}$ appropriate to the repeat distance and continues well beyond it. Clearly, one would have to utilize a great deal of imagination to accept these curves as giving one very much information about the observed repeat distances.

Since the experimentally interesting region extends out to about 50 monolayers, Eq. (7) must be evaluated for large z. Long-range effects arise much more easily from discontinuities in the slope of $\chi(\mathbf{q})$: They will give oscillatory contributions which drop off as z^{-2}. This shows up very clearly in a most illustrative manner if one attmpts to evaluate $I(z)$ utilizing a simple Folin integration scheme to account for the rapid variation of the cosine. The results thus obtained are actually determined by the integration mesh since the Folin integration scheme approximates the remaining integrand by a series of quadratic polynomials which join continuously but with discontinuous slope at alternate mesh

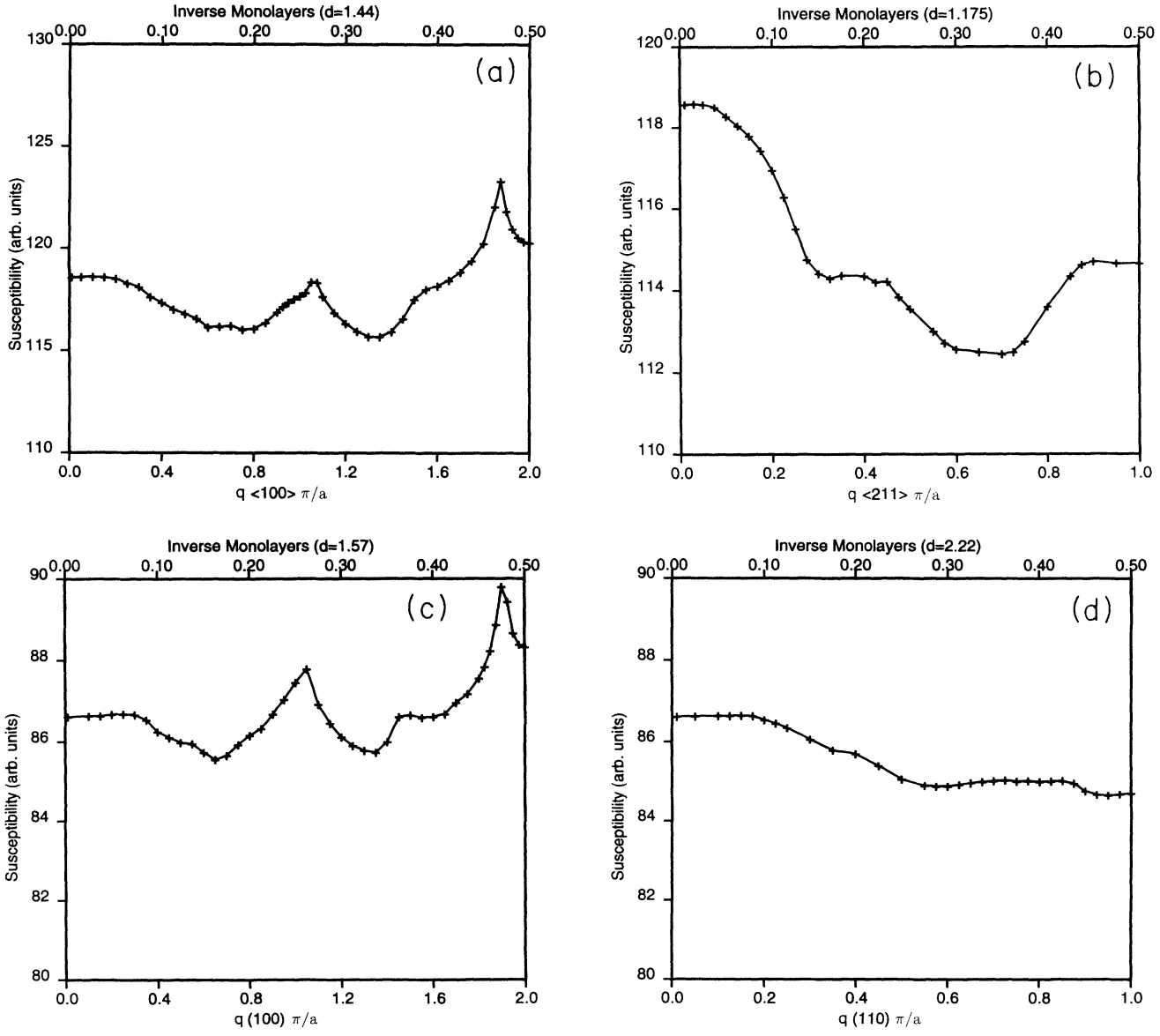

FIG. 4. Generalized susceptibility $\tilde{\chi}(\mathbf{q})$ for (a) Cr (100), (b) Cr (211), (c) Mo (100), and (d) Mo (110).

points. The spurious large z oscillations generated result from the presence of those cusps as can be easily demonstrated by direct integration. Actual slope discontinuities are precisely what are generated by the Kohn anomalies which are pairs of points calipering the Fermi surface with oppositely directed velocities. This exercise is a vivid illustration for the student of the significance of Kohn anomalies. Their effects on phonon spectra have been extensively studied and the method to graphically present them is the same.[32] Of course, it is to be expected that actual peaks in the susceptibility will be more robust towards the degradations of impurities, strains, and temperature. They can be of interest, however, only if extremely sharp (unlikely), strongly enhanced in a bootstrap fashion, or perhaps to provide the near field behavior in the response.

D. Kohn-anomaly analysis

The RKKY analysis of Roth, Zeiger, and Kaplan[76] is extended to the planar configuration.[4] Focus is restricted to only those contributions to I which give oscillatory behavior because a significant sized space relating the boundary between occupied and unoccupied states (i.e., the Fermi energy) can be found with the same $\mathbf{q}$ vector . One has a nonoscillatory component I_0, which is neglected, plus a sum of oscillatory components:

$$I(z) = I_0(z) + \sum I^{\alpha}_{Ka}(z)\,, \tag{8}$$

where each I^{α}_{Ka} contribution is derived from the expansion about a pair of k points on the Fermi surface with oppositely directed velocities. α labels an indexing of the caliper point pairs $\{\mathbf{k^0}, n; \mathbf{k^{0'}}, n'\}$ on the Fermi surface.

$$I^{\alpha}_{Ka}(z) = \frac{-Z(\mathbf{k}^0_{\|}, (k^{0'}_z - k^0_z))}{2(2\pi)^4} \int d\mathbf{k}_{\|} \int dk_z \int dk'_z\; e^{iz(k'_z - k_z)} \left(\frac{f_n(\mathbf{k}_{\|}, k_z) - f_{n'}(\mathbf{k}_{\|}, k'_z)}{\epsilon_n(\mathbf{k}_{\|}, k_z) - \epsilon_{n'}(\mathbf{k}_{\|}, k'_z)} \right). \tag{9}$$

The integration limits are $\pm\pi/d$ for the k_z and k'_z integrations and over the 2D BZ of the plane for the $\mathbf{dk}_{\|}$ integration. The $\mathbf{q}$ dependence of the matrix elements incorporated in Z can be neglected for a much broader class of assumed interactions in Eq. (9) since they are generally much more slowly varying than the energy factor of the integrand. Thus Z has been evaluated at the caliper points and brought out of the integrations. The energy is to be locally expanded to quadratic order about the Fermi energy

$$\epsilon = \mathbf{v} \cdot \delta\mathbf{k} + \delta\mathbf{k} \cdot \overleftrightarrow{D} \cdot \delta\mathbf{k}/2\,, \tag{10}$$

from which one will extract $\delta k_z(\epsilon, \delta\mathbf{k}_{\|})$. One can choose to set up the quadratic coefficient matrix $\overleftrightarrow{D}$ as a symmetric matrix which simplifies the development. As the boundaries make no interesting contribution to this analysis, the limits will be approximated as infinite. The evaluation of $I^{\alpha}_{Ka}(z)$ requires that the $\mathbf{z}$ quadratic term $(D_{zz}k_z)$ be negligible across $(|v_z|^{-1}T)$ — which is a diagonal of the thin shell selected by the Fermi factor. So, shifting origin so the δ's are no longer needed for $\mathbf{k}_{\|}$,

$$k_z(\mathbf{k}_{\|}, \epsilon) = k^o_z + \frac{\epsilon - \mathbf{v} \cdot \mathbf{k}_{\|} - \frac{1}{2}\mathbf{k}_{\|} \cdot \overleftrightarrow{D} \cdot \mathbf{k}_{\|}}{v_z(\mathbf{k}_{\|})}\,, \tag{11}$$

where

$$v_z(\mathbf{k}_{\|}) = v_z + \hat{\mathbf{z}} \cdot \overleftrightarrow{D} \cdot \mathbf{k}_{\|}\,. \tag{12}$$

With this, one converts the k_z and k'_z integrations to energy integrations which are continued into the complex plane as contour integrals. The only poles are those due to the Fermi factors which results in summing the contributions of the residues which is a geometric series. The contour integration also reinforces the requirement that the velocities must be antiparallel — but not necessarily along $\hat{\mathbf{z}}$ — to get a nonzero contribution. The integrand of the $\mathbf{k}_{\|}$ integration is denoted as $B_{\alpha}(\mathbf{k}_{\|})$,[4] and is

$$B_{\alpha}(\mathbf{k}_{\|}) = \frac{2\pi F_{\alpha}(z,T) e^{iq^{\alpha}_z z}}{z[|v'_z(\mathbf{k}_{\|})| + |v_z(\mathbf{k}_{\|})|]} + \text{c.c.}\,, \tag{13}$$

with the temperature broadening factor obtained from the residue sum

$$F_{\alpha}(z,T) = \frac{z/L_{\alpha}(T)}{\sinh[z/L_{\alpha}(T)]}\,, \tag{14}$$

which involves a coherence length

$$L_{\alpha}(T) = \frac{v^{\alpha}_z(\mathbf{k}_{\|})}{2\pi T}\,. \tag{15}$$

It is here that the utility of the RKKY formulation will be exploited since it is quite natural to consider replacing T by $(T+T^*)$ where T^* represents additional Fermi surface broadening due to alloying, strains, etc. (One could even go so far as to call T^* a Dingle-Robinson temperature.) q^{α}_z has the expected definition

$$q^{\alpha}_z(\mathbf{k}_{\|}) = k'_z(\mathbf{k}_{\|}, 0) - k_z(\mathbf{k}_{\|}, 0)\,. \tag{16}$$

But the effective velocity is an inverse of the average of inverses:

$$(v^{\alpha}_z)^{-1}(\mathbf{k}_{\|}) = [v'^{-1}_z(\mathbf{k}_{\|}) + v^{-1}_z(\mathbf{k}_{\|})]/2\,. \tag{17}$$

Note that as $T \to 0$, $L_{\alpha} \to \infty$ indicating no thermal scattering limiting the range of the coherence and consequently $F_{\alpha} \to 1$.

The remaining $(\mathbf{k}_{\|})$ integration must be performed to determine the strength and functional dependence of the decay. It is evaluated using the stationary phase approximation. The stationary phase requirement enforces the need to be at a Kohn-anomaly caliper and is the basis for the de Haas–van Alphen analogy.[29] The first step is

to expand $q_z^\alpha(\mathbf{k}_\parallel)$ to second order in $\mathbf{k}_\parallel$:

$$q_z^\alpha(\mathbf{k}_\parallel) = q_{zo}^\alpha + \frac{1}{v_z'}\left(\frac{\mathbf{v}'\cdot\mathbf{k}_\parallel}{v_z'}\hat{\mathbf{z}} - \frac{1}{2}\mathbf{k}_\parallel\right)\cdot\overleftrightarrow{D}'\cdot\mathbf{k}_\parallel - \frac{1}{v_z}\left(\frac{\mathbf{v}\cdot\mathbf{k}_\parallel}{v_z}\hat{\mathbf{z}} - \frac{1}{2}\mathbf{k}_\parallel\right)\cdot\overleftrightarrow{D}\cdot\mathbf{k}_\parallel . \quad (18)$$

The linear term is zero in this expression as a consequence of the velocities being antiparallel. The 2×2 matrix can now be made diagonal through a rotation, and so

$$q_z^\alpha(\mathbf{k}_\parallel) = q_{z0}^\alpha + \frac{k_x^2}{\kappa_x^\alpha} + \frac{k_y^2}{\kappa_y^\alpha}, \quad (19)$$

which returns us to the notation of Bruno and Chapert albeit with a somewhat more complex expression in Eq. (18). This results from choosing to include the expansion of $v_z(\mathbf{k}_\parallel)$ in the denominator of Eq. (11). The κ's appearing in Eq. (19) are the effective mass eigenvalues whose geometric mean determine the plane parallel component of the local joint density of states. The remaining integration over the parallel (in-plane) coordinates then gives

$$I_{Ka}^\alpha(z) = \frac{-Z(\mathbf{0}, q_{z0}^\alpha)}{z^2} m_\alpha^* F_\alpha(z,T)\sin(q_{z0}^\alpha z + \psi_\alpha), \quad (20)$$

where m_α^* is basically a local joint density of states given by

$$m_\alpha^* = \frac{2|\kappa_x^\alpha\kappa_y^\alpha|^{1/2}}{|v_z| + |v_z'|} = \frac{|\kappa_x^\alpha\kappa_y^\alpha|^{1/2} v_z^\alpha}{|v_z v_z'|} \quad (21)$$

and ψ_α is a phase that is $0, \pi/2, \pi$ for a local maximum, saddle point, or minimum. Note that the v_z terms in the denominator of m_α^* represent the plane perpendicular contribution to the local joint density of states.

A more careful consideration of the $\mathbf{k}_\parallel$ integration is useful. The $1/z^2$ factor in Eq. (20) arises from the $1/z$ factor in B_α plus a $1/z$ factor due to the $\mathbf{k}_\parallel$ integration. This is the result for a point singularity where both κ's in Eq. (19) are finite, and so the Gaussian integrals in each direction both contribute a $1/\sqrt{z}$ factor. But for the other extreme of perfect planar nesting, both κ's would be infinite and the integration over the parallel (in-plane) coordinates would instead be done for a constant phase over some finite region and contribute no such factor. In that case, the $1/z$ would not be obtained from the $\mathbf{k}_\parallel$ integration, and so the strength of the interaction decays more slowly as $1/z$. For a line of coincidence, only one of the κ's would be infinite and the dependence would be $1/z^{3/2}$. Thus, if no other factors are operative, the rate of decay can yield information as to the nature of the singularity. This difference and the κ factors in m_α^* deal with variation in the 2D BZ, i.e., parallel to the layers. F_α, should it become significant, and the v_z appearing in the denominator of m_α^* represent variations perpendicular to the layers. This distinction will enter the discussion shortly.

One can locate these Kohn-anomaly caliper points in many ways. The technique employed here starts by using local linear expansions of the energy bands within tetrahedral microzones to divide the Fermi surface up into a series of platelets. These were then checked pairwise to locate regions of possible caliper points — clearly such an approach cannot locate them. Then, returning to the Fourier spline fit representation, a steepest descent search was made for the caliper point. The imprecision of the linear expansions caused many platelet pairs to be mapped to the same caliper, and so duplicates had to be eliminated. A better approach would be to utilize a quadratic expansion within the tetrahedra. This would actually give approximate calipers which could then be refined. Once the caliper point is located, the effective mass parameter (m_α^*) is calculated by determining the velocities and second derivative $\overleftrightarrow{D}$ matrices using finite differences (definitely a weak point in the procedure but adequate to our use), performing the required rotations, and then evaluating Eq. (21). The results for these Kohn-anomaly Fermi surface caliper points are best presented by bar plots giving the strength as the height of the bar placed at the $\mathbf{q}$ vector where it occurs.[32,31] The strength is a product of m_α^* with the number of times the same caliper occurs due to symmetry (i.e., the degeneracy). Each bar is labeled with an S (saddle point), m (minimum), or M (maximum). One can believe those marked S but m and M can get interchanged according to whether a reciprocal lattice vector or reflection has been incorporated. This was not well tracked.

1. Nb

Figure 5 gives the results for Nb along the (110) direction using the calculation incorporating the empirical p-d shift. The same calculation was also done without that p-d shift. It produced only one significant change: The saddle point singularity at the experimentally observed 0.25 inverse layers instead occurs much closer to 0.2 inverse layers if the shift is not applied. This is of some interest since the the observed repeat distance is 4 ML.[59] Incorporating spin-orbit coupling had no significant effect. At first glance, this result looks quite promising in that this caliper occurs at a $\mathbf{q}$ of 0.245 inverse layer repeat distance and is only exceeded in strength by one at a 10 layer repeat distance — which would be severely decayed before it could be observed. However, note here that there is another caliper at a $\mathbf{q}$ of 0.268 inverse layers. This will become important in the next section since this (smaller) m caliper is one of the few calipers involving significant s-p character in the associated wave functions. A significant factor in the increased strength of the S caliper is its fourfold degeneracy whereas the m caliper only occurs once. Otherwise the S caliper would only be about 50% stronger. The location of these two calipers is shown in Fig. 6(a). The S caliper arises from the four vectors reaching from the octahedron around Γ to the arms of the jungle gym. The m caliper arises from spanning the ellipses — it only has a weight of one in spite of there being two arrows because they occur at the surface of the BZ.

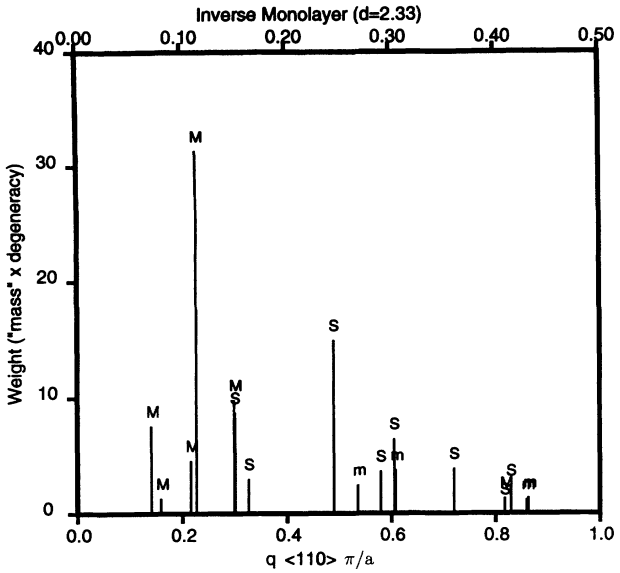

FIG. 5. Kohn-anomaly caliper points for Nb along the (110) direction. The *d-p* shift shifts the saddle point found at 0.25 inverse layers to its current position from a location nearer 0.2 inverse layers. For convenience, a **q** coordinate in terms of inverse layers has been included on the top of the plot.

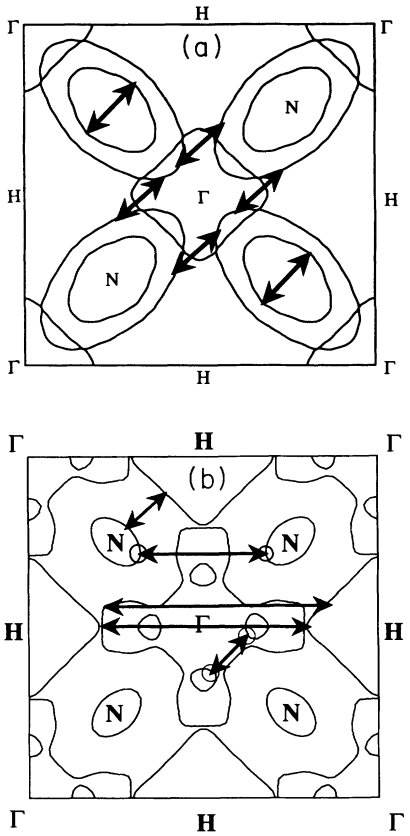

FIG. 6. Base plane ($k_z = 0$) Fermi surfaces on an expanded scale for (a) Nb and (b) Mo. Nb has three Fermi surface sheets: the octahedron centered on Γ, the ellipses centered on N, and the jungle gym which in this plane looks like a larger set of ellipses truncated. The four caliper vectors near Γ would correspond to a **q** of 0.245 inverse layers. The vector spanning the ellipses would correspond to a **q** of 0.268 inverse layers. Mo has four Fermi surface sheets: the jack centered on Γ, the octahedron centered on H, the lens found along the Δ line from Γ to H, and the (smaller) ellipses centered at N. Mo has two caliper from the jack to the octahedron and one from ellipse to ellipse near the appropriate 3 ML repeat distance. It is the ellipses at N that contain what *s-p* character occurs at the Fermi surface in both these two materials.

2. *Cr*

Results for the same cases shown in Fig. 4 are shown in the same order in Fig. 7. Not surprisingly, the results for Cr (100) are dominated by a cluster of calipers just below the 2 ML repeat distance at the end of the zone. This requires some interpretation, however, since that **q** vector is known to be a region of planar nesting. Because the codes used are designed to find *points* in a sharply differential sense with no widths, they will always find *points* based on the small variations in the representation — or else fail. Thus, a cluster of many points is indicative of some greater degree of nesting. Should this occur for a caliper of interest, further investigation is in order since the degree of nesting influences the rate of decay. For Cr, the situation near the H point is known to be full planar nesting, and so the decay should occur as $1/z$. The history of theoretical understanding of the spin density wave is that first the strong peak in the generalized susceptibility arising from this nesting was discovered;[77] then it was shown that that peak was washed out by matrix element effects in the noninteracting susceptibility [Eq. 3]; and finally it was shown that the exchange enhancement reestablished it.[75] Because of the restricted variational freedom allowed in their calculation, the results of van Schilfgaarde and Herman[22] demonstrate most clearly that the exchange enhancement is not an essential feature for the multilayers containing Cr as a spacer. Matrix elements still act to reduce the strength of the nesting, but perhaps not as strongly as in the bulk spin density wave case. The boundary conditions acting to form a quantum well state may help to stabilize the response in this case. Note, however, that this calculation also gives another cluster of points near the 4 ML repeat distance (a harmonic apparently unobserved) in agreement with the generalized susceptibility calculations. This set of points is a mixture of differing band index combinations and so not a nesting and would not have the slower decay rate.

As for the long period oscillation, if any caliper is going to relate to the 18 Å, or 12.5 ML, repeat distance, then it must come from the smallest calipers indicated in Fig. 7. The three smallest calipers all arise from the band 5 lens which occurs along the Δ line inside the neck of the jack. The lens is formed as a result of the interaction between the Γ centered octahedron and the mid-Δ centered knob. Consequently, the jack is formed on the one hand and the lens on the other. The Fermi surface drawings of Sparlin and Marcus[78] for Mo are a useful reference since the paramagnetic Cr and Mo Fermi surfaces are qualitatively similar and the lens is not usually discussed for Cr. They

are also visible in Fig. 6(b). The smallest caliper corresponds to about a 10.5 ML repeat distance. Its effective mass factor is only 0.75 with a degeneracy of 2, and so, on the very large scale used to accommodate the nesting vectors, it does not show up. The calculational techniques were not designed to look closely at this problem. An adjustment of the Fermi energy within its uncertainties can, in fact, bring it into agreement with the 18 Å repeat distance. The wave function character involved on the lens is interesting, being the result of the (anti)crossing of the downward sweeping $(3z^2 - r^2)$ type e_g band with the upward sweeping xy member of the t_{2g} d states. For this reason, van Schilfgaarde and Harrison[79] reject the lens as the origin of this long wavelength on the basis that the matrix elements will be null. For the caliper found along Γ-H, this matrix element issue is quite germane: The matrix elements involved for the bulk susceptibility will definitely be null. Of course, such arguments may be indicative but they are far less applicable for the multilayers. However, the actual spanning vector they considered spans the lens from rim to rim perpendicular to the Γ-H line (an apparent misquote of Stiles). This vector is slightly larger — without adjustment, the calculation corresponds to a repeat distance of 8 ML with an effective mass of 0.68 and a degeneracy of 4. In the rim of the lens, the wave function character is mixed t_{2g} and e_g and the matrix element argument does not apply. The phase space (degeneracy × effective mass) is actually a little better for this rim caliper although, clearly, both are weak.

The significance of the lenses is heightened by long repeat distances found in other directions. In the (211)

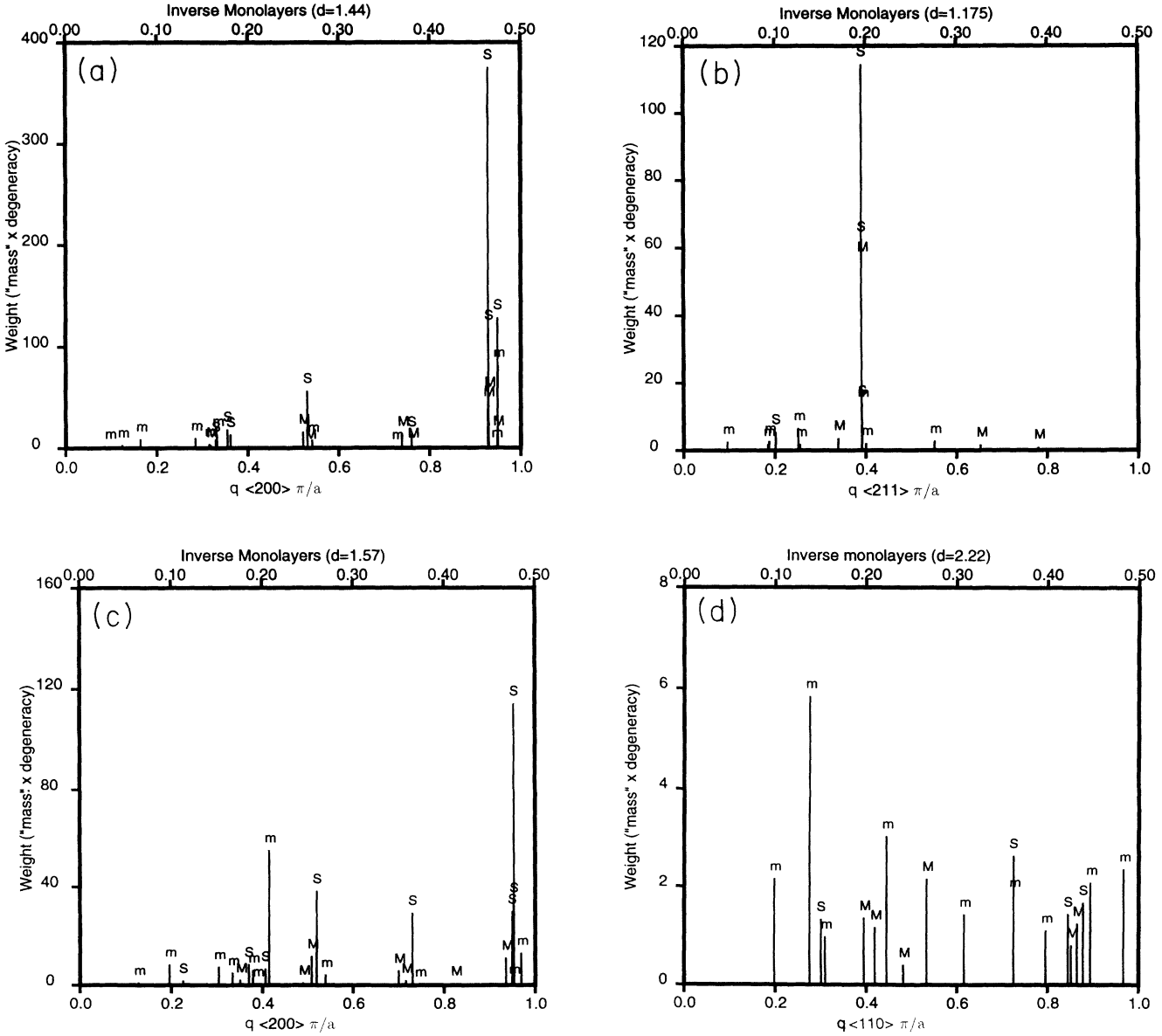

FIG. 7. Kohn-anomaly caliper points for (a) Cr (100), (b) Cr (211), (c) Mo (100), and (d) Mo (110). For convenience, a **q** coordinate in terms of inverse layers has been included on the top of the plot.

direction, the repeat distance is found to also be an 18 Å long oscillation period with the same strength and phase.[54] The smallest caliper shown in Fig. 7(b) corresponds to a near-rim caliper with repeat distance of about 10.5 ML. With a layer separation of 1.175 Å rather than 1.44 Å, that distance is the same as that found for the rim caliper. The effective mass is small (0.64 with a degeneracy of 4), just as for the (100) direction. Even more, although not universally agreed upon, it appears that a Cr (110) spacer also exhibits an 18 Å repeat distance. If one accepts this, arguments based on aliasing for the 2 ML repeat distance in the (100) direction require very careful reexamination and are unlikely to prove robust. It also places a very stringent requirement on any explanation involving lens spanning vectors: The spanning vector must be of identical length in all three directions. The (100) and (110) equivalence is easily accommodated if the spanning vector is on the rim while the (211) is on a (001) to (110) rotation rather than the required (001) to (100) rotation. However, the calculations show it to slide near a rim to rim connection with nearly identical caliper length and effective mass. Because the rim of the lens is one side of an anti-crossing — the other side being the neck of the jack — it is not as well represented using the band-by-band Fourier series spline representation of the current study. Use of experimental data would be the best approach. Unfortunately, experimental information on the lens is not readily available for Cr. But, for isoelectronic Mo, although the lens is extended along the transverse (100) directions,[80] these distortions[78] are only about 3%. The size cannot be taken from Mo data but the indications of constant length are very credible. If the (100) spanning vector were to instead be along the Γ-H direction, one would necessarily find an angular variation which, though small, would probably be larger than the stringent limits placed by experiment. The evidence for the rim caliper being the relevant one is quite strong.

One last comment should be made about the (211) direction: The dominant feature seen in Fig. 7(b) is the collection of points all at 0.20 inverse layers (= 5 ML) — which are indeed a full planar nesting and should exhibit a $1/z$ decay. That such a repeat distance is not seen experimentally implies either materials limitations or small coupling strength. These results indicate that much could be learned by attempting to improve sample perfection and looking for a 6 Å repeat distance.

3. Mo

The (100) direction for Mo [Fig. 7(c)] looks very much like a fuzzy version of the Cr (100) plot. Which is entirely consistent with the generalized susceptibilities (Fig. 4). Of particular significance is that the strong nesting near the outside boundary of the BZ is weakened due to the poorer coincidence of the two Fermi surface pieces. This is probably the cause that the 2 ML repeat distance is not observed since one can assume that the strength is just barely adequate in Cr, matrix element and exchange factors being less likely. While the matrix element effects act more strongly to suppress this peak in the bulk,[61] they should be very comparable for the multilayers involving as they do the iron form factor. And since it appears that the exchange enhancement is not playing a significant role even for Cr, it should definitely not be a consideration for Mo. Differing surface roughness can be a factor: While the material can be prepared to very high quality, the greater lattice mismatch probably also implies a greater surface roughness. This would also act to kill the 2 ML repeat. Further information can be obtained from dHvA measurements in Mo[81] where it is reported that the signals for the electron jack were extremely weak. Since this repeat distance involves the coupling of jack and octahedron states, that observed weakness should imply a weak interlayer coupling.

Interestingly, Mo also has clusters of caliper points appropriate for 3, 4, and 5 ML repeat distances all with roughly comparable strengths. Without a knowledge of the other pieces of the problem, all a Kohn-anomaly tabulation can do is provide a list of possibilities. It is annoying when the list is too inclusive. The hint of a growing predilection for a 3 ML repeat distance does appear in the generalized susceptibility, though. Since the 3 ML repeat distance is what is seen experimentally, the appropriate spanning vectors are shown in Fig. 6(b). The two vectors connecting the jack centered on Γ to the octahedron centered on H have zero matrix elements in the bulk susceptibility whether using the more approximate tight binding[31] or the full LAPW (this work) basis set to represent the wave functions. While the appropriate matrix elements for Z would be different, they would have some of the same dependences, and so one can expect that the contribution of these calipers would also be reduced — reservations against carrying such arguments too far have already been given. The weak strength of the jack states observed from the dHvA measurements for the 2 ML repeat distance also apply here. Those two vectors correspond to a 3 ML repeat distance although they are actually longer than the nesting vectors that drive the 2 ML repeat distance. That is because they combine with a $\frac{2\pi}{a}(100)$ reciprocal lattice vector to yield the shorter vector — an example of aliasing. The remaining caliper connects between the N-centered ellipses and actually has the smallest mass factor (0.48 with a degeneracy of 4). These N-centered ellipses are the only surfaces which contain significant s-p character. That will be seen to be significant in the next section.

The remaining panel for the (110) direction of Mo fully illustrates the frustrating aspect of the Kohn-anomaly-type analysis. About all it tells you is that anything is possible. If one instead looks backwards and examines the calipers with $\mathbf{q}$'s for an 0.2 inverse repeat distance (= 11 Å), one can gain some useful insight. Two calipers occur very close together: one at a $\mathbf{q}$ for 0.21 inverse layers and one for almost precisely 0.20. The one at 0.21 connects the body of the Γ-centered jack to the N-centered ellipse. It has an effective mass of 0.58 with a degeneracy of 2. The other has a mass of 0.68 also with a degeneracy of 2. It, however, has another interesting feature in that it is a vector interconnecting the lenses out along Δ. This would be consistent with the long repeat distance

found in Cr by involving the same Fermi surface piece. It is thus tempting to hypothesize that the little lens surface is particularly favorable as a carrier of the magnetic information.

III. MODELING THE IMPERFECT SYSTEM

The experimentally realizable systems are not the perfect system assumed in the simplest model. The focus of this statement is not on the problems of the interfaces (and their effects incorporated through the factor Z) but on the imperfect crystalline character of the spacer itself. That is not to imply that the interfaces are not very important but instead to merely scope the problem. Given that there is a lattice mismatch and a work function (read charge) mismatch across the interface in almost all systems, it is not surprising that the spacer should exhibit a wide variety of inhomogeneous strains, dislocations, etc. Further, the rigors of preparing the system make it very difficult to provide the quality achieved in bulk single crystal studies. These limiting factors will all act to destroy phase coherence, and so it is not surprising that these macroscopic quantum oscillations should appear only in the most favorable cases.

A useful feature of the transmission-medium treatment discussed in the previous section is that it suggests a simple extension for the imperfect system. Following the approach used by people studying the temperature variation of RKKY interactions in rare earths, one merely inserts a scattering length; actually, the easiest way to proceed in this case is to introduce a Dingle-Robinson-like temperature. That is, one replaces T by $(T + T^*)$ in Eq. (15) for the coherence length L_α where T^* is basically an inverse effective scattering time reflecting the Fermi surface broadening about the two end points of the caliper. One could extract information to make some estimates for T^* from alloy calculations but the primary interest is in strain effects rather than the substitutional impurities normally studied. However, it is extremely tempting to assume that inhomogeneous strains will produce effects varying in a similar manner as those of the substitutional impurities since the essential feature is localized (d's) versus delocalized (s-p's). dHvA studies for substitutional impurities in Mo[81,82] indicate that the Dingle temperatures are approximately constant over all pieces of the Fermi surface *but* that it is a factor of 2 smaller on the N-centered ellipses. (The results for the N ellipses are calculational since experimental limitations precluded an accurate experimental determination.) This is precisely what is assumed by people doing high temperature transport calculations.

Insight can be gained from a simplified simulation. The asymptotic analysis being made is only applicable for "large z" and $z/L_\alpha \to 0$. T^* must be small or L will be reduced from its assumed infinite size to a value where z/L_α is large. The F_α factor would then become significant and introduce a damping factor which would be approximately an exponential decay. One can now introduce the idea that the s and p states will scatter far less than the d states and the oscillations involving the s-p states will persist but those involving d states will be damped out. Accordingly, one examines a revised weight factor that multiplies the (mass $\times$ degeneracy) weight by the fractional s-p character at each end of the caliper vector. The s-p character is estimated considering only the wave function character within the muffin tin sphere (which will underestimate the relative amount of s-p character). Since only qualitative insight is sought, it is adequate. Because the groups VB and VIB materials are predominantly d character at the Fermi energy, such a procedure will drastically reduce the possibilities predicted strongly favoring the N-centered ellipses. The two interesting cases are shown in Fig. 8.

One other point offers an interesting possibility. L_α has the effective velocity v_z^α in the numerator. Obviously, the scattering (T^*) can be much larger and not reduce

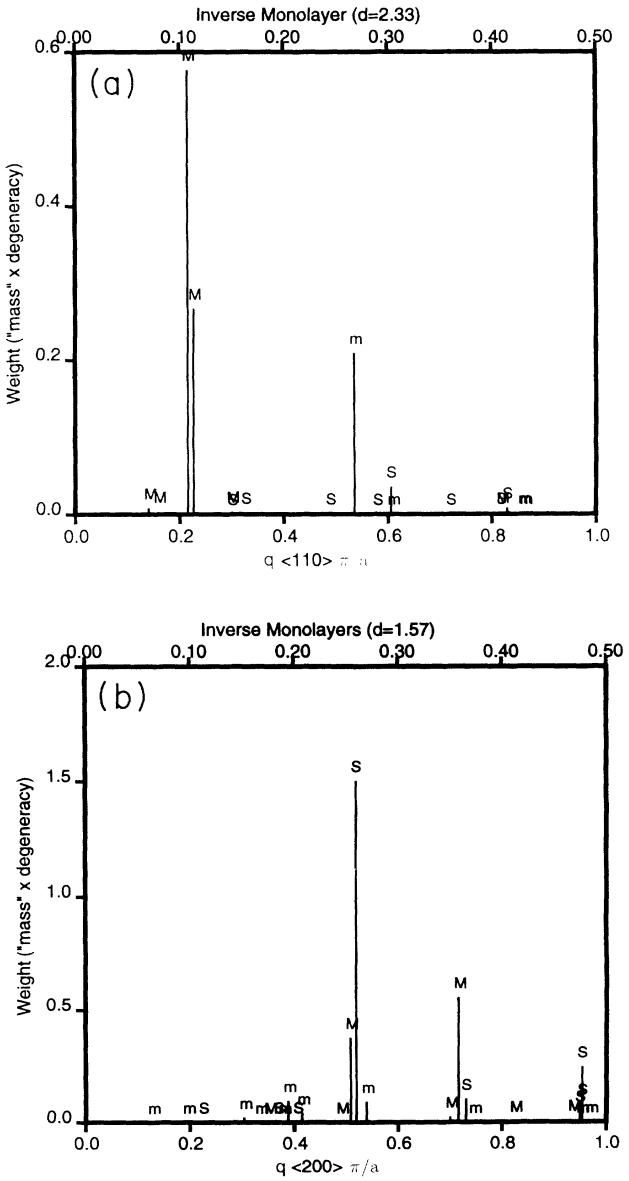

FIG. 8. s-p weighted Kohn-anomaly caliper points for (a) Nb (110), (b) Mo (100). The s-p weighting is to simulate the effect of the imperfect spacer as discussed in the text.

the size of L_α if the effective velocity is also much larger. This is closely related to the empirical observation that when dHvA measurements are made on less perfect samples, it is the small, light mass Fermi surfaces which can still be seen. (An interesting consequence of this possibility is that the X pockets in the heavier transition metals might be favored surfaces for producing the spanning vectors observed.) In the case of the caliper vectors, what this means is that one would like to have nesting or near nesting — i.e., large inverse curvature factors κ — but also large velocities. The large velocities will help *increase* the size of the coherence length but will *decrease* the size of the effective mass parameter m^*_α . This is the probable origin of the fact that there is very little correlation of the observed frequencies to the weights given in Figs. 5 and 7. Because the s-p states also have larger velocities, the same two cases of Fig. 8 are the ones with the large effective velocities as shown in Fig. 9.

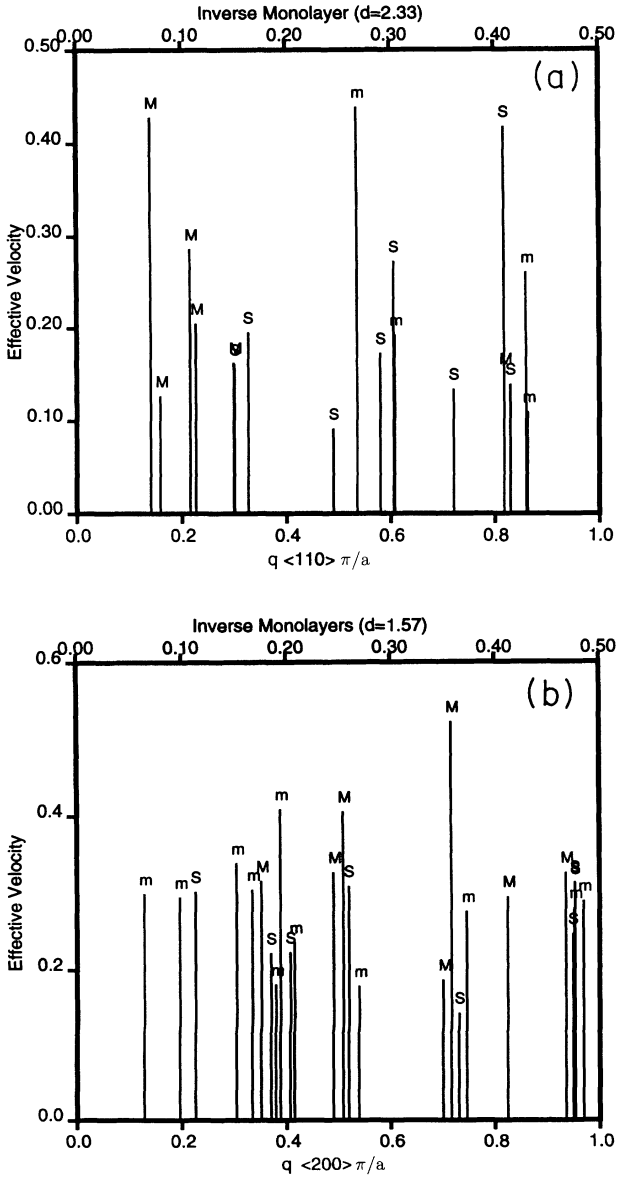

FIG. 9. Effective velocities of the Kohn-anomaly caliper points for (a) Nb (110), (b) Mo (100).

A. Nb

In the Nb (110) direction, only the 4 and 10 ML repeat distances remain but no further distinction can be made between these persisting calipers on the basis of their wave function character: The two calipers at 10 ML span the ellipse while the caliper at 4 ML spans from one ellipse to another, and so they both contain s-p character. However, from the effective velocities [Fig. 9(a)], one sees that the 4 ML repeat distance has the significantly larger effective velocity. So the picture can be made consistent. One other interesting feature is the disappearance due to this construction of the saddle point (S) caliper that was sensitive to the empirical d shift. That caliper involved the Γ-centered piece, which in Mo would be the electron jack, and so its vanishing could be considered consistent with the weak dHvA signals reported for the Mo jack.

B. Mo (100)

For Mo in the (100) direction, only the 3 and 4 ML repeat distances remain. The 2 and 5 ML repeat distances have been eliminated. One can even push the analysis farther. The persisting 4 ML repeat distance only remains because the wave function at one end of the spanning vector is very strongly of s-p character and, using this crude index, it makes up for the very weak s-p character at the other end. The repeat distance couples the N-centered ellipse with the knob of the Γ-centered jack. The jack wave function only has about 5% s-p character mixed into the wave function. It seems unlikely that such a caliper could persist. (Note the weak signal of the jack occurring again.) On the other hand, the retained caliper at 3 ML connects two N-centered ellipses with both wave functions involved about 2/3 s-p character; and, as seen in Fig. 9(b), its velocity is roughly twice the mean velocity of the other calipers. Here, too, it would appear that the picture can be considered quite consistent. As a footnote, it can be added that preliminary calculations for the perfect Fe/Mo system do find the 2 ML repeat distance instead.[83]

C. Mo (110) and Cr

This analysis does not explain, nor is it applicable to, either Mo (110) or Cr where it has already been established that the calipers involve d states. In the case of the 2 ML short wavelength (100) oscillation of Cr, the relevant feature is that the lattice mismatch is small and the material of very high quality — not the incipient antiferromagnetism. For a very high quality system, the arguments given above for requiring s-p character or high effective velocity do not as clearly apply. Although the interfaces may be rougher for the 18 Å repeat distances seen in Cr, the lattice mismatch is no worse. One can expect scattering not to be such a strong issue in those cases just as in the case of the 2 ML repeat distance. This probably also is the case for Mo in the (110) orientation — which, though textured, is of extremely high

quality. So examining the effects of scattering is not as informative for these systems.

One can, however, make an interesting prediction for Cr in the (100) direction. If the material quality — not the interface alone — were to be degraded, then one would expect the same 3 ML repeat distance as for Mo (100). The *s-p* selection of the *N*-centered ellipses due to reduced scattering is just as strong and the enhancement of the effective velocity for that caliper is even more pronounced. By finding a magnetic layer with significant lattice mismatch, one would expect this 3 ML repeat distance to replace the 2 ML distance.

IV. DISCUSSION

The intent of this work was to focus as much as possible on the spacer as a transmission medium. The natural consequence is that the basic analysis is a tabulation of Fermi surface calipers associated with Kohn anomalies in phonon spectra. When the project was initiated, a primary intent was to demonstrate that the resulting list of possible repeat distances would be so exhaustive as to be uninteresting. That expectation was fully realized for these three materials. The local joint density of states represented as an effective mass parameter has been seen to have marginal, if any, predictive power as to which possible repeat distance will actually be present. For the simple model system, nothing has been done here to improve that situation.

A great deal of progress can be made for the Nb and Mo spacer systems by realizing that they are not very perfect systems due to significant lattice mismatch, and so it is necessary to account for scattering. One approach is to minimize the scattering effects (minimize T^*) which can be achieved by selecting states with significant *s-p* character. This proved useful for Nb (110) and Mo (100). (The predominance of *s-p* character in Cu makes such considerations far less significant for Cu, as well as for the other noble and simple metals.) In Cr, the exchange enhancement proves not to be the significant factor but, instead, it is the greater material quality achievable that makes it special. Thus the Cr (100) short period appears at 2 ML in spite of the fact that it involves mostly *d* character. The reduced nesting coupled with the lattice mismatch producing an inhomogeneous (scattering) system selects against the *d* states of the jack and octahedron thereby eliminating the 2 ML repeat distance in Mo and also eliminates the 4 and 5 ML response that would otherwise occur. This provides an explanation for Mo exhibiting a 3 ML repeat distance. Changing the magnetic layer to induce lattice mismatch should cause Cr to also exhibit a 3 ML rather than 2 ML repeat distance.

The calipers involving significant *s-p* character are also more resistant to dephasing by scattering because their effective velocities are generally larger. The requirement is for large effective velocity, not that the states be of *s-p* character, and so it could occur for *d* states as well. A large effective velocity (to reduce dephasing) will — except in the case of nesting or near nesting — correspond to reduced effective mass (or phase space). This offers an explanation for the local joint density of states (effective mass m_α^*) demonstrating very little predictive power. If scattering is not as damaging for calipers with high velocities, it will cause the system to select them, and retain coherence, over those with larger effective mass, and increase phase space.

s-p selectivity also helps understand the predominance of repeat distances in the 9–11 Å range and the increased strength of the coupling towards the right-hand side of the transition series. The main arguments for this predominance are, of course, the observational difficulties for the long periods and the cutoffs for short periods produced by form factors and roughness. *s-p* selectivity also selects for $\mathbf{q}$'s in the middle regions of the BZ. One near constant for transition metals is that they have roughly one nearly free electron (NFE or *s-p*) because the *d*-bands position in the middle of the NFE band slowly sinking to accommodate the additional *d* electrons as one proceeds across the series. This is the significance of the name transition series. The result is that the *s-p* character will show up nearer the middle of the BZ. The argument is weak but observations from the data shown and a great deal not shown here suggest that it is indeed the case. As for the coupling strength increasing towards the right-hand side of the transition series, observe that the Fermi energy is moved out of the Fano antiresonance as the number of electrons is increased.

The calipers involving the lenses in Mo and Cr involve a different mechanism since the wave functions involved are of very nearly pure *d* character. Little can be said other than to note that the calipers involve the rim of the lens where the $t_{2g}(m_\ell = \pm 2)$ state is mixing with the $e_g(m_\ell = 0)$ state. Accepting the hypothesis that these calipers are robust, then Mo (110) becomes consistent with the uniform long wavelength oscillations for Cr in the (100), (211), and (110) directions.

One feature that could be looked at more carefully to understand the properties of the spacer as a transmission medium is the decay of the coupling strength. The simple geometrical aspects of the Kohn-anomaly calipering are already of interest: a $1/z^2$ decay being appropriate to a point singularity, a $1/z^{3/2}$ decay appropriate to a line of singularities, and a $1/z$ to full planar nesting. Can such 3D continuum results be carried over to the finite sized multilayers with any utility? Certainly it is only valid in the large z regime — which is all the approach can be used for. Then, can one also detect F_α effects? The phase, on the other hand, should primarily be a property of the interface and interesting as such.

What is to be made of this argument that the site density being different within the planes and perpendicular to the planes can induce a signal from a reflected position in the BZ? This would only apply to the (100) direction of Cr. Because one would need a structured interaction to induce an umklapp-type interaction as well as an interface-blurring interaction, the effect would be moderately weak. One would need a strong instance of the effect for it to be observed. That strong instance could,

of course, best be the nesting observed in Cr. However, because the long oscillation is observed in multiple directions, this effect very probably cannot be its primary explanation. But does it contribute in the Cr (100) direction? The answer lies in the rate of decay because a "reflected interaction" would retain the slower decay rate. One cannot claim to see much evidence of that in the data [although the coupling is stronger at large distances in the (100) direction than in the (211) direction]. So this is probably an interesting idea yet without an application.

ACKNOWLEDGMENTS

This work was initiated as the result of discussions with J. Mattson and S. D. Bader. It has greatly profited from a continuing dialogue with them as well as with E. Fullerton. The communication prior to publication of the results for the ideal Mo spacer by S. Mirbt is much appreciated. The work was supported by the U.S. Department of Energy under Contract No. W-31-109-ENG-38 and a grant of computer access at the National Energy Research Supercomputer Center.

[1] P. Grünberg, R. Schreiber, Y. Pang, M. B. Brodsky, and C. H. Sowers, Phys. Rev. Lett. **57**, 2442 (1986).
[2] S. S. P. Parkin, N. More, and K. P. Roche, Phys. Rev. Lett. **64**, 2304 (1990).
[3] Y. Yafet, J. Appl. Phys. **61**, 4058 (1987).
[4] P. Bruno and C. Chappert, Phys. Rev. B **46**, 261 (1992); Phys. Rev. Lett. **67**, 1602 (1991).
[5] M. N. Baibich, J. M. Broto, A. Fert, F. Nguyen Van Dau, F. Petroff, P. Eitenne, G. Creuzet, A. Friederich, and J. Chazelas, Phys. Rev. Lett. **61**, 2472 (1990).
[6] G. Binasch, P. Grünberg, F. Saurenbach, and W. Zinn, Phys. Rev. B **39**, 4828 (1989).
[7] R. E. Camley and J. Barnás, Phys. Rev. Lett. **63**, 664 (1989).
[8] J. Barnás, A. Fuss, R. E. Camley, P. Grünberg, and W. Zinn, Phys. Rev. B **42**, 8110 (1990).
[9] R. Q. Hood and L. M. Falicov, Phys. Rev. B **46**, 8287 (1992); L. M. Falicov and R. Q. Hood, J. Magn. Magn. Mater. **121**, 362 (1993).
[10] K. Ounadjela, C. B. Sommers, A. Fert, D. Stoeffler, F. Gautier, and V. L. Moruzzi, Europhys. Lett. **15**, 875 (1991).
[11] F. Herman, J. Sticht, and M. van Schilfgaarde, J. Appl. Phys. **69**, 4783 (1991).
[12] D. Stoeffler, K. Ounadjela, and F. Gautier, J. Magn. Magn. Mater. **93**, 386 (1991).
[13] D. Stoeffler and F. Gautier, Prog. Theor. Phys. Suppl. **101**, 139 (1990); Phys. Rev. B **44**, 10 389 (1991); J. Magn. Magn. Mater. **104-107**, 1819 (1992); **121**, 259 (1993).
[14] H. Hasegawa, Phys. Rev. B **42**, 2368 (1990).
[15] J.-H. Xu and A. J. Freeman, Phys. Rev. B **47**, 165 (1993).
[16] T. Jarlborg and A. J. Freeman, J. Appl. Phys. **53**, 8041 (1982).
[17] E. Bruno and B. L. Gyorffy, J. Magn. Magn. Mater. **121**, 322 (1993); Phys. Rev. Lett. **71**, 181 (1993).
[18] Y. Wang, P. M. Levy, and J. L. Fry, Phys. Rev. Lett. **65**, 2732 (1990).
[19] P. M. Levy, S. Zhang, and A. Fert, Phys. Rev. Lett. **65**, 1643 (1990).
[20] P. M. Levy, Z.-P. Shi, S. Zhang, H. E. Camblong, and J. L. Fry, J. Magn. Magn. Mater. **121**, 357 (1993).
[21] S. S. P. Parkin, Phys. Rev. Lett. **71**, 1641 (1993).
[22] M. van Schilfgaarde and F. Herman, Phys. Rev. Lett. **71**, 1923 (1993).
[23] J. E. Inglesfield, J. Phys. C **10**, 3141 (1977).
[24] P. Lang, L. Nordström, R. Zeller, and P. H. Dederichs, Phys. Rev. Lett. **71**, 1927 (1993).
[25] S. Mirbt, H. L. Skriver, M. Aldén, and B. Johansson, Solid State Commun. **88**, 331 (1993).
[26] R. P. Erickson, K. B. Hathaway, and J. R. Cullen, Phys. Rev. B **47**, 2626 (1993).
[27] E. Bruno, J. Magn. Magn. Mater. **116**, L13 (1992).
[28] E. Bruno, J. Magn. Magn. Mater. **121**, 248 (1993).
[29] D. M. Edwards, J. Mathon, R. B. Muniz, and M. S. Phan, J. Phys. Condens. Matter **3**, 4941 (1991); Phys. Rev. Lett. **67**, 493 (1991).
[30] J. Mathon, M. Villeret, D. M. Edwards, and R. B. Muniz, J. Magn. Magn. Mater. **121**, 242 (1993).
[31] M. D. Stiles, Phys. Rev. B **48**, 7238 (1993).
[32] P. L. Taylor, Phys. Rev. **131**, 1995 (1963).
[33] D. Pescia, D. Kerkmann, F. Schumann, and W. Gudat, Z. Phys. B **78**, 475 (1990).
[34] S. S. P. Parkin, R. Bhadra, and K. P. Roche, Phys. Rev. Lett. **66**, 2152 (1991).
[35] M. Johnson, S. T. Purcell, N. W. E. McGee, R. Coehoorn, J. ann de Stegge, and W. Hoving, Phys. Rev. Lett. **68**, 2688 (1992).
[36] Z. Q. Qiu, J. Pearson, and S. D. Bader, Phys. Rev. B **46**, 8659 (1992).
[37] B. Heinrich, Z. Celinski, J. F. Cochran, W. B. Muir, J. Rudd, Q. M. Zhong, A. S. Arrot, K. Myrtle, and J. Kirschner, Phys. Rev. Lett. **64**, 673 (1990).
[38] W. R. Bennett, W. Schwarzacher, and W. F. Egelhoff, Jr., Phys. Rev. Lett. **65**, 3169 (1990).
[39] A. Fuss, S. Demokritov, P. Grünberg, and W. Zinn, J. Magn. Magn. Mater. **103**, L221 (1992).
[40] J. E. Ortega, F. J. Himpsel, G. J. Mankey, and R. F. Wills, Phys. Rev. B **47**, 1540 (1993).
[41] C. Carbone, E. Vescovo, O. Rader, W. Gudat, and W. Eberhardt, Phys. Rev. Lett. **71**, 2805 (1993).
[42] K. Garrison, Y. Chang, and P. D. Johnson, Phys. Rev. Lett. **71**, 2801 (1993).
[43] F. Y. Fradin, Phys. Rev. Lett. **33**, 158 (1974); F. Y. Fradin, D. D. Koelling, A. J. Freeman, and T. J. Watson-Yang, Phys. Rev. B **12**, 5570 (1975).
[44] P. G. de Gennes, J. Phys. Rad. **23**, 510 (1962); P. G. de Gennes and D. Saint-James, Solid State Commun. **1**, 62 (1965).
[45] D. C. Mattis, *The Theory of Magnetism* (Harper and Row, New York, 1965).
[46] A. J. Heeger, A. P. Klein, and P. Tu, Phys. Rev. Lett. **17**, 803 (1966).
[47] J. A. Blackman and R. J. Elliot, J. Phys. C **3**, 2066 (1970).
[48] K. Grobsky and B. N. Harmon, J. Appl. Phys. **49**, 2147 (1978).
[49] J. J. Krebs, P. Lubitz, A. Chaiken, and G. A. Prinz, Phys. Rev. Lett. **63**, 1645 (1989).
[50] S. F. Alvarado and C. Carbone, Physica B **149**, 43 (1988).
[51] J. Unguris, R. J. Celotta, and D. T. Pierce, Phys. Rev.

Lett. **67**, 140 (1991).
[52] S. O. Demokritov, J. A. Wolf, and P. Grünberg, Appl. Phys. Lett. **63**, 2147 (1993).
[53] Z. Q. Qiu, J. Pearson, and S. D. Bader, J. Appl. Phys. **73**, 5765 (1993).
[54] E. E. Fullerton, M. J. Conover, J. E. Mattson, C. H. Sowers, and S. D. Bader, Phys. Rev. B **48**, 15 755 (1993).
[55] M. E. Brubaker, J. E. Mattson, C. H. Sowers, and S. D. Bader, Appl. Phys. Lett. **58**, 2306 (1991).
[56] S. S. P. Parkin, Phys. Rev. Lett. **67**, 3598 (1991).
[57] Z. Q. Qiu, J. Pearson, A. Berger, and S. D. Bader, Phys. Rev. Lett. **68**, 1398 (1992).
[58] P. J. H. Bloemen, W. J. M. de Jonge, and R. Coehoorn, J. Magn. Magn. Mater. **121**, 306 (1993).
[59] J. E. Mattson, C. H. Sowers, A. Berger, and S. D. Bader, Phys. Rev. Lett. **68**, 3252 (1992).
[60] Z.-P. Shi, P. M. Levy, and J. L. Fry, Phys. Rev. Lett. **69**, 3678 (1992).
[61] K. Schwartzman, J. L. Fry, and Y. Z. Zhao, Phys. Rev. B **40**, 454 (1989).
[62] F. Herman and R. Schrieffer, Phys. Rev. **46**, 5806 (1992).
[63] J. Callaway, A. K. Chatterjee, S. P. Singhal, and A. Ziegler, Phys. Rev. B **28**, 3818 (1983).
[64] L. Hedin and B. I. Lundqvist, J. Phys. C **4**, 2064 (1971).
[65] D. G. Shankland, in *Computational Methods in Band Theory*, edited by P. Markus, J. Janak, and A. Williams (Plenum, New York, 1971), p. 362.
[66] D. D. Koelling and J. H. Wood, J. Comput. Phys. **67**, 253 (1986).
[67] W. E. Pickett, H. Krakauer, and P. B. Allen, Phys. Rev. B **38**, 2721 (1988).
[68] J. Rath and A. J. Freeman, Phys. Rev. B **11**, 2109 (1975).
[69] J. Harris and R. O. Jones, J. Chem. Phys. **68**, 3316 (1978).
[70] J. G. Harrison, J. Chem. Phys. **79**, 2265 (1983); **78**, 4562 (1983).
[71] J. G. Harrison, R. A. Heaton, and C. C. Lin, J. Phys. B **16**, 2079 (1983).
[72] G. W. Crabtree, D. H. Dye, D. P. Karim, and D. D. Koelling, Phys. Rev. Lett. **42**, 390 (1979).
[73] N. Elyashar and D. D. Koelling, Phys. Rev. B **15**, 3620 (1977); **13**, 5362 (1976).
[74] R. Blaschke, J. Ashkenazi, O. Pictet, D. D. Koelling, A. T. van Kessel, and F. M. Mueller, J. Phys. F **14**, 175 (1984).
[75] E. Fawcett, Rev. Mod. Phys. **60**, 209 (1988).
[76] L. M. Roth, H. J. Zeiger, and T. A. Kaplan, Phys. Rev. **149**, 519 (1966).
[77] W. M. Lomer, Proc. Phys. Soc. London **80**, 489 (1962); **84**, 327 (1964).
[78] D. M. Sparlin and J. A. Marcus, Phys. Rev. **144**, 484 (1966).
[79] M. van Schilfgaarde and W. A. Harrison, Phys. Rev. Lett. **71**, 3870 (1993).
[80] G. B. Brandt and J. A. Rayne, Phys. Rev. **132**, 1945 (1963).
[81] A. J. Arko and F. M. Mueller, Phys. Condens. Matter **19**, 231 (1975).
[82] H. W. Myron and F. M. Mueller, Phys. Condens. Matter **19**, 241 (1975).
[83] S. Mirbt (private communication).

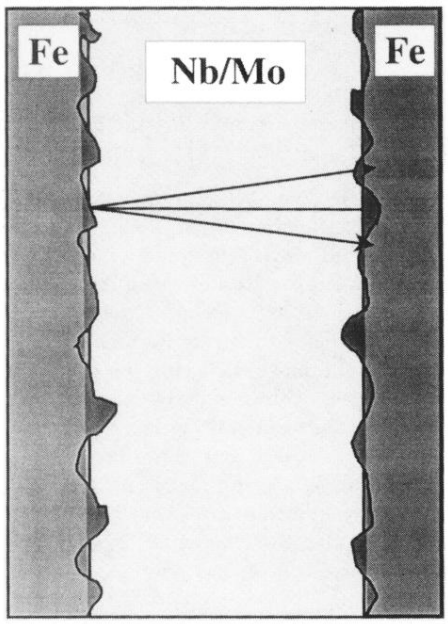

FIG. 1. Schematic representation of the multilayer system. Two layers of iron are coupled through the Nb/Mo spacer — which is initially viewed as a simple transmission medium. The boundaries, which are generally not perfect, are approximated as perfect interfaces to which corrections are applied. The figure misrepresents the relative size of the length scales for the variations along and perpendicular to the interfaces. One can expect the scale along the interface to be longer than shown. Not represented are the larger-scaled imperfections such as interdiffusion and strains.